

A nodal model for co-condensation synthesis of silicide nanoparticles using inductively coupled thermal plasmas

M. Shigeta¹, T. Watanabe²

¹*Department of Mechanical Systems and Design, Tohoku University, Sendai, Japan*

²*Department of Environmental Chemistry and Engineering, Tokyo Institute of Technology, Yokohama, Japan*

Abstract: In this study, our previous co-condensation model is improved with the concept of nodal discretization for the size space in order to clarify the growth mechanism of silicide nanoparticles in an inductively coupled thermal plasma reactor. When the silicon content in the feed powders is 66.7 %, nanoparticles of MSi_2 ($M=Mo, Ti$) are fabricated as the main product. Nanoparticles of Ti_5Si_3 are mainly synthesized in the case of the silicon content 33.0 %. These results show good agreement with the experiment.

Keywords: Inductively coupled thermal plasma, Nanoparticle, Silicide, Aerosol, Nodal model

1. Introduction

It is known that nanoparticles of silicides show unique characteristics such as high electrical conductivity and high heat/oxidation resistance [1]. In particular, disilicides of molybdenum $MoSi_2$ and titanium $TiSi_2$ have been expected to be applied to solar control windows, electromagnetic shielding, and electrodes for Very Large Scale Integration (VLSI). In addition, fabrication of the other type of silicide such as Ti_5Si_3 is also required since it has substitutional alloying possibilities and potential for ductile phase toughening as well as a high melting point [2].

An inductively coupled thermal plasma (ICTP) can be considered as a useful tool for synthesis of those functional nanoparticles with the precise control of the particle size distribution and the corresponding stoichiometric composition [3-11]. Furthermore, mass production of them has been expected to be accomplished by an ICTP operated at atmospheric pressure, because an ICTP provides several advantages such as large energy density, high chemical reactivity, variable properties, large plasma volume, as well as long residence/reaction time. Its unique thermofluid field can promptly vaporize a large amount of raw materials even with high melting/boiling points. Moreover, effective fabrication of nanoparticles is simultaneously achieved by nucleation and condensation in a highly supersaturated state owing to the rapid cooling at the tail of an ICTP.

However, the practical synthesis of the silicide nanoparticles by an ICTP is a complicated phenomenon including the field interaction with numerous variables. The nanoparticles of silicides are synthesized through co-condensation of multi-component vapors in a few milliseconds [12, 13]. In addition, the growth mechanism is dependent on the properties of silicon and the other metal. In order to clarify the growth mechanism and to control the process effectively, the experimental study has been carried out [14]. Furthermore, in our previous numerical study [12], a multi-component co-condensation model was proposed. However, neither the growth by coagula-

tion between nanoparticles nor the thermophoretic effect was considered.

In the present study, our previous model is improved with the more general formula covering all range of Knudsen number to estimate the growth rate by heterogeneous co-condensation more accurately. Moreover, the effects of coagulation and thermophoresis are taken into account. In order to numerically solve the governing equation of the nanoparticle growth, the concept of nodal discretization for the size space is adopted [15]. As a result, the improved multi-component co-condensation model with nodal discretization is proposed and applied to the practical condition of the synthesis to elucidate the growth mechanism of silicide nanoparticles in an ICTP reactor. Mo-Si system and Ti-Si system are investigated particularly focusing on the fabrication of nanoparticles of $MoSi_2$, $TiSi_2$, and Ti_5Si_3 .

2. Modeling

The thermofluid fields and the electromagnetic fields in the ICTP are conventionally determined by solving the two-dimensional conservation equations of mass, momentum, energy and concentration coupled with the Maxwell's equations.

$$\nabla \cdot (\rho \mathbf{u}) = 0 \quad (1)$$

$$\rho \mathbf{u} \cdot \nabla \mathbf{u} = -\nabla p + \nabla \cdot \boldsymbol{\tau} + \mathbf{J} \times \mathbf{B} \quad (2)$$

$$\rho \mathbf{u} \cdot \nabla h = \nabla \cdot \left(\frac{\lambda}{C_p} \nabla h \right) + \mathbf{J} \cdot \mathbf{E} - \dot{q}_r \quad (3)$$

$$\rho \mathbf{u} \cdot \nabla Y = \nabla \cdot (\rho D \nabla Y) + R_r \quad (4)$$

$$\nabla^2 \mathbf{E} - \eta_0 \sigma_e \frac{\partial \mathbf{E}}{\partial t} = 0 \quad (5)$$

where ρ is the density, \mathbf{u} is the velocity, p is the pressure, $\boldsymbol{\tau}$ is the viscous stress tensor, \mathbf{J} is the conductive current, \mathbf{B} is the magnetic flux density, h is the enthalpy, λ is the thermal conductivity, C_p is the specific heat at constant pressure, \mathbf{E} is the electric field

intensity, \dot{q}_r is the radiation loss per unit volume, Y is the mass fraction, D is the diffusion coefficient, R_r is the net production rate, η_0 is the magnetic permeability, σ_e is the electrical conductivity, and t is the time.

The precursor particles with a few micrometer diameters are injected into the plasma as the raw materials. The motion of the single in-flight particle is described by

$$m_p \frac{d\mathbf{u}_p}{dt} = \frac{\pi}{8} d_p^2 \rho C_D (\mathbf{u} - \mathbf{u}_p) |\mathbf{u} - \mathbf{u}_p| + m_p \mathbf{g} \quad (6)$$

where m is the mass, d is the diameter, C_D is the drag coefficient, \mathbf{g} is the gravity, and the subscript p denotes particle. The temperature history of the single particle is obtained by solving the equation of energy balance considering heat transfer due to the plasma flow and the radiation loss.

$$\pi d_p^2 [\dot{q}_{plasma} - \varepsilon_p \sigma_{St} (T_p^4 - T_a^4)] = \begin{cases} \frac{\pi}{6} \rho_p d_p^3 c_p \frac{dT_p}{dt} & (T_p < T_m, T_m < T_p < T_b) \\ \frac{\pi}{6} \rho_p d_p^3 H_m \frac{dx_f}{dt} & (T_p = T_m) \\ -\frac{\pi}{2} \rho_p d_p^2 H_b \frac{d(d_p)}{dt} & (T_p = T_b) \end{cases} \quad (7)$$

where ε is the emissivity, σ_{St} is Stephan-Boltzmann constant, T is the temperature, T_a is the ambience temperature, c is the specific heat, and x_f is the fraction of liquid phase. H_m and H_b correspond to the latent heats at the melting point T_m and the boiling point T_b , respectively. When the continuum-flow model becomes no longer applicable in the evaporation process with the decrease in the particle diameter, the heat transfer is treated in a free molecular regime.

For the computation of nanoparticle synthesis, the concept of nodal discretization is adopted [15]. In the nodal model, the particle size space is discretized into nodes and the formed particles reside only at the nodes. To cover the wide range of particle sizes, the nodes are spaced linearly on a logarithmic scale.

$$v_{pk+1} = f_q v_{pk} \quad (k=1, 2, \dots, k_{max}) \quad (8)$$

where v_p is the volume of the particle, and f_q is the geometric spacing factor. The subscript k represents the node number.

The governing equation for the particle concentration N_p at the node k is given by the general dynamic equation for aerosol [16].

$$\frac{dN_{pk}}{dt} = [\dot{N}_{pk}]_{nucl} + [\dot{N}_{pk}]_{coag} + [\dot{N}_{pk}]_{cond} \quad (9)$$

The each term of the right-hand side represents the net production rate. The subscripts *nucl*, *coag*, and *cond* stand for nucleation, coagulation, and condensation, respectively [15, 17].

$$[\dot{N}_{pk}]_{nucl} = \sum_m I_m \xi_k^{nucl} \quad (10)$$

$$[\dot{N}_{pk}]_{coag} = \frac{1}{2} \sum_i \sum_j \xi_{ijk}^{coag} \beta_{ij} N_{pi} N_{pj} - N_{pk} \sum_i \beta_{ik} N_{pi} \quad (11)$$

$$[\dot{N}_{pk}]_{cond} = \sum_i \frac{(\xi_{ik}^{cond} - \delta_{ik}) N_{pi}}{\Delta t} \quad (12)$$

where I is the homogeneous nucleation rate, ξ is the size operator, β is the collision frequency function, δ is the Kronecker delta.

The growth rate owing to heterogeneous co-condensation is estimated from the net molecular flux covering all range of Knudsen number Kn [18]

$$\frac{dv_{pi}}{dt} = \sum_m 2\pi d_{pi} D_{vapm} v_{1m} (n_{1m} - n'_{s_{1m}}) \times \left[\frac{0.75\alpha_m (1 + Kn_i)}{0.75\alpha_m + 0.283\alpha_m Kn_i + Kn_i + Kn_i^2} \right] \quad (13)$$

where d_p is the particle diameter, n is the concentration, α_m is the accommodation coefficient of the species m , and D_{vap} represents the diffusion coefficient of the vapor. The subscripts 1 and S denote monomer and the saturation state, respectively. The concentration in the saturated state is modified by considering Kelvin effect.

3. Numerical results

Figure 1 shows a schematic illustration of the nanoparticle synthesis system consisting of a plasma torch and a reaction chamber. The operating conditions and torch geometry are given in Table 1.

Figure 2 (a) and figure 3 (a) show the evolution of the particle number density for Mo-Si system and Ti-Si

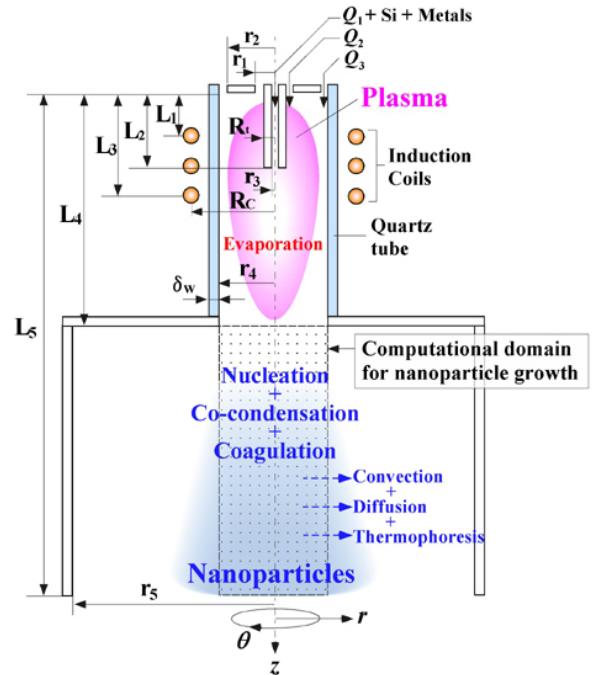


Fig. 1 Nanoparticle synthesis system.

Table 1 Geometry and operating conditions.

Outer radius of inner slot (r_1):	6.5 mm
Outer radius of outer slot (r_2):	21.0 mm
Inner radius of injection tube (r_3):	1.0 mm
Inner radius of torch (r_4):	22.5 mm
Inner radius of chamber (r_5):	100.0 mm
Outer radius of injection tube (R_t):	4.5 mm
Radius of coils (R_C):	32.0 mm
Distance to frontal end of coil (L_1):	19.0 mm
Insertion length of probe (L_2):	45.0 mm
Distance to rear end of coil (L_3):	65.0 mm
Torch length (L_4):	190.0 mm
Distance to end of chamber (L_5):	380.0 mm
Input power:	5.0 kW
Applied frequency:	4.0 MHz
Coil turn number:	3
Operating pressure:	101.3 kPa
Wall thickness (δ_w):	1.5 mm
Flow rate of career gas (Q_1):	1.0 Sl/min
Flow rate of plasma gas (Q_2):	3.0 Sl/min
Flow rate of sheath gas (Q_3):	30.0 Sl/min
Powder feed rate:	0.1-0.3 g/min
Si content in feed powders:	25-80 at.%

system respectively. Figure 2 (b) and figure 3 (b) present the evolution of the silicon content in the synthesized nanoparticles for Mo-Si system and Ti-Si system respectively. The dashed lines indicate the moment when the formation of the nuclei by nucleation is still more dominant than the nanoparticle growth by condensation and coagulation. The growth by condensation and coagulation overcomes nucleation, as the nanoparticles are transported downstream.

In Mo-Si system, the profile begins to have a peak in figure 2 (a) when the silicon vapor starts to condense on the molybdenum nanoparticles. In heterogeneous condensation, less vapor can condense on smaller nanoparticles due to the rarefied gas effect with larger Knudsen numbers. Thus, the profile passes into the bimodal distribution around $z = 230.0$ mm. However, the first peak of the smaller nanoparticles gradually disappears owing to the consumption of the smaller nanoparticles by coagulation. Figure 2 (b) tells that larger amount of silicon vapor condenses on the larger nanoparticles until condensation process finishes. After that, the nanoparticles slowly grow by coagulation. Figures 2 (a) and (b) indicate that the nanoparticles with the diameters larger than 10 nm approach the stoichiometric composition.

On the other hand in Ti-Si system in figure 3 (a), a large number of nuclei are generated at the early stage $z = 228.0$ mm, and immediately coagulation process becomes more effective. Thus, the profile does not show a remarkable bimodal distribution since the smaller nanoparticles are easily consumed for growth. Because of the simultaneous co-condensation of the vapors of silicon and

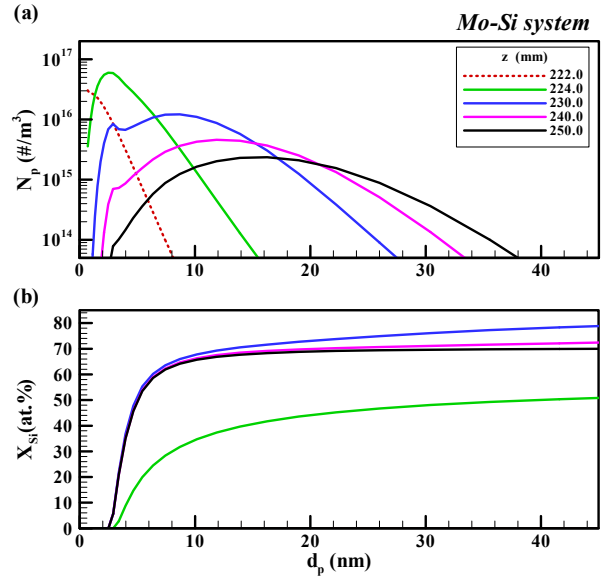


Fig. 2 Size/composition profiles of nanoparticles for Mo-Si system: (a) Particle number density, (b) Silicon content.

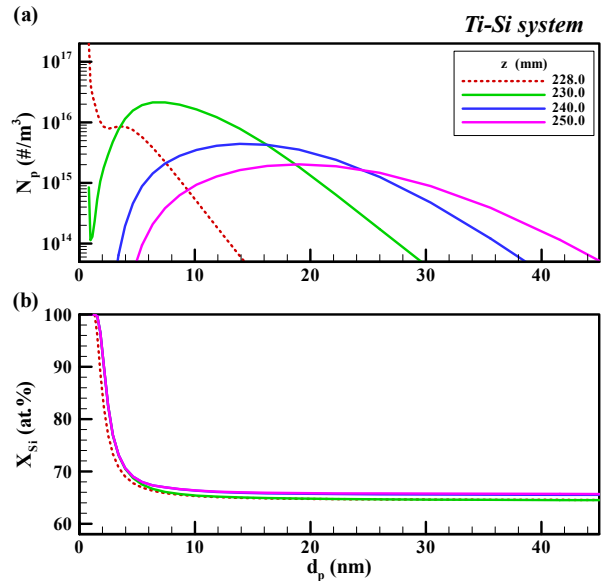


Fig. 3 Size/composition profiles of nanoparticles for Ti-Si system: (a) Particle number density, (b) Silicon content.

titanium, the profiles of the silicon content keep identical as shown in figure 3 (b).

Figures 4 (a) and (b) compare the particle size distribution function obtained from the present model with that obtained from the experimental study [14, 17] for both systems. These results show good agreements in both Mo-Si system and Ti-Si system, which validates the present model for the nanoparticle growth.

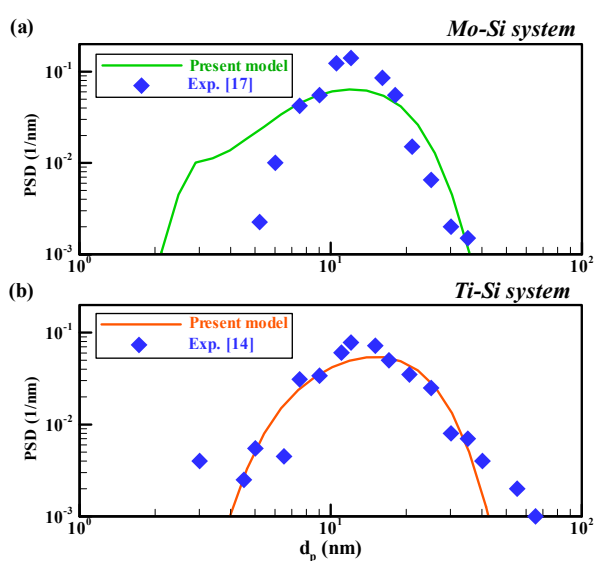


Fig. 4 Particle size distribution functions: (a) Mo-Si system, (b) Ti-Si system.

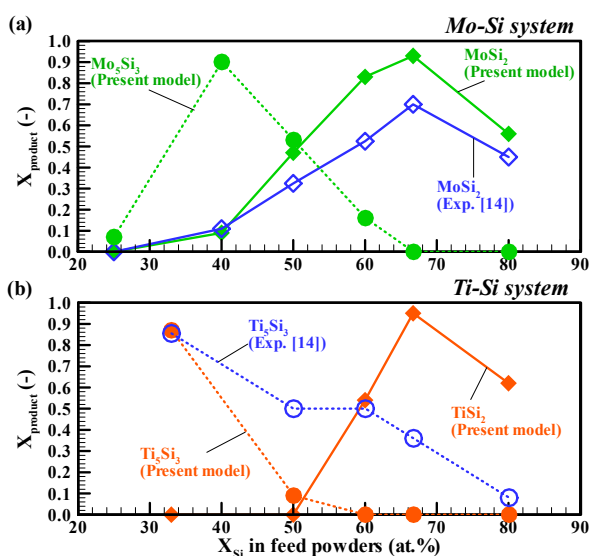


Fig. 5 Relative content of the compounds: (a) Mo-Si system, (b) Ti-Si system.

Figure 5 gives the comparison of the present numerical and experimental results concerning the relative contents of the compounds for the different silicon content in the feed powders [14]. For MoSi_2 , these results also show good agreement as shown in figure 15 (a). This guarantees that the nanoparticles of the disilicide MoSi_2 are successfully synthesized when the silicon content in the feed powders is 66.7 at.%. In addition, the present computation shows that the nanoparticles of Mo_5Si_3 are mainly synthesized in the case of the initial silicon content of 40.0 at.%. In figure 15 (b) about Ti-Si system, Ti_5Si_3 displays the similar tendencies between the computation and the experiment. Particularly in the case 33.0 at.% of the initial

silicon content, the relative content obtained from the present model quantitatively agrees with the experimental result very well. Therefore, the present model expresses the growth mechanism of the silicide nanoparticles with respect to the composition as well.

References

- [1] K. Matsuura, T. Hasegawa, T. Ohmi, M. Kudoh, *Metal Mater. Trans. A* **31-3**, 747 (2000).
- [2] J. Williams, PHD thesis, Iowa state univ. **IS-T 1898**, (1999).
- [3] Japan Society of Mechanical Engineers, *Functional Fluids and Intelligent Fluids* (Tokyo, Corona Pub. Corp.), 2000.
- [4] S.L. Girshick, C.-P. Chiu, R. Muno, C.Y. Wu, L. Yang, S.K. Singh, P.H. McMurry, *J. Aerosol Sci.* **24-3**, 367 (1993).
- [5] J.F. Bilodeau, P. Proulx, *Aerosol Sci. and Tech.* **24**, 175 (1996).
- [6] M. Desilets, J.F. Bilodeau, P. Proulx, *J. Phys. D: Appl. Phys.* **30**, 1951 (1997).
- [7] T. Watanabe, K. Fujiwara, *Chemical Engineering Communication* **191-10**, 1343 (2004).
- [8] M. Shigeta, T. Watanabe, H. Nishiyama, *Thin Solid Films* **457**, 192 (2004).
- [9] T. Watanabe, A. Nezu, Y. Abe, Y. Ishii, K. Adachi, *Thin Solid Films* **435**, 27 (2003).
- [10] M. Shigeta, T. Watanabe, *JSME International Journal B* **48**, 425 (2005).
- [11] M. Shigeta, T. Watanabe, *Transactions of ASME, Journal of Heat Transfer* **127**, 1222 (2005).
- [12] M. Shigeta, T. Watanabe, *J. Mater. Research* **20**, 2801 (2005).
- [13] M. Shigeta, T. Watanabe, *Thin Solid Films* **515**, 4217 (2007).
- [14] T. Watanabe, H. Okumiya, *Sci. and Tech. of Advanced Materials* **5**, 639 (2004).
- [15] Prakash A, Bapat AP and Zachariah MR 2003 A simple numerical algorithm and software for solution of nucleation, surface growth, and coagulation problems *Aerosol Sci. and Tech.* **37** 892-98.
- [16] S.K. Friedlander, *Smoke, Dust and Haze, Fundamentals of Aerosol Dynamics* 2nd Ed. (New York, Oxford Univ. Press), 2000.
- [17] M. Shigeta, T. Watanabe, *J. Phys. D: Appl. Phys.* **40**, 2407 (2007).
- [18] J.H. Seinfeld, S.N Pandis, *Atmospheric Chemistry and Physics, From Air Pollution to Climate Change* (New York, John Wiley & Sons, Inc.), 1998.